



ELSEVIER

Ultrathin entrance windows for silicon drift detectors

R. Hartmann^{a,*}, L. Strüder^a, J. Kemmer^b, P. Lechner^b, O. Fries^c, E. Lorenz^c, R. Mirzoyan^c

^aMPI Halbleiterlabor, Paul-Gerhardt-Allee 42, D-81245 München, Germany

^bKETEK GmbH, Am Isarbach 30, D-85764 Oberschleißheim, Germany

^cMax-Planck-Institut für Physik, Föhringer Ring 6, D-80805 München, Germany

Abstract

Detectors with ultrathin entrance windows have been fabricated, which show an overall improvement of the detector performance in the optical and X-ray region as well as for heavy ions. The quantum efficiency was higher than 60% within the entire wavelength range between 200 nm and 800 nm. In the soft X-ray region the spectroscopic resolution could be improved significantly. For the $Mn_{K\alpha}$ line a peak to valley ratio of 5700:1 was achieved. Measurements with ^{241}Am α -particles revealed an effective “dead” layer width of less than 150 Å.

The compatibility of the technology to produce thin entrance windows with the planar process allows its application on various pn-junction detector designs. A new silicon drift detector with a total area of 21 mm² was successfully tested and operated at count rates up to 3×10^7 s⁻¹ cm⁻². At room temperature, the devices have shown an energy resolution for the $Mn_{K\alpha}$ line of 227 eV (FWHM) with shaping times of 250–500 ns, decreasing to 152 eV at –20°C. The fast readout in combination with a large detector area, a homogeneous entrance window and an exceptionally low noise without the need of an extensive cooling system makes them especially suited for spectroscopic applications in non-laboratory environments.

1. Introduction

Backside illuminated pn-junction detectors, like the silicon drift chamber shown in Fig. 6 or pn-CCD's [3], consist of a fully depleted n-type bulk with a p⁺-rear contact, acting as the radiation entrance window. The unstructured rear pn-junction combined with a fully depleted bulk results in detector structures with a high quantum efficiency over a wide range of energy and an excellent spatial homogeneity. In addition, modifications in the implantation technology for the p⁺-rear contact have only little effect on the detector process in general.

The net doping profile and resulting electric field of our standard p⁺-implantation are shown in Fig. 2a. The pn-junction is situated at a depth of approximately 280 nm. Photons in the UV- and soft X-ray region with short absorption lengths in silicon (see Fig. 1) are absorbed in an almost field free, highly doped region. Therefore, photo-generated signal charges are lost by recombination with a high probability.

To reduce the width of this partially insensitive area, the process technology for the p⁺-entrance window implanta-

tion was optimized. The implantation of boron ions through a SiO₂ layer gives a resulting doping profile, which is shifted towards the detector surface (see Fig. 2b). The SiO₂ layer is removed afterwards. While the position of the pn-junction is placed at a depth of 40–50 nm, the integrated hole concentration underneath the detector surface is high enough to guarantee the functionality of the detector at full depletion. Due to the Poisson equation

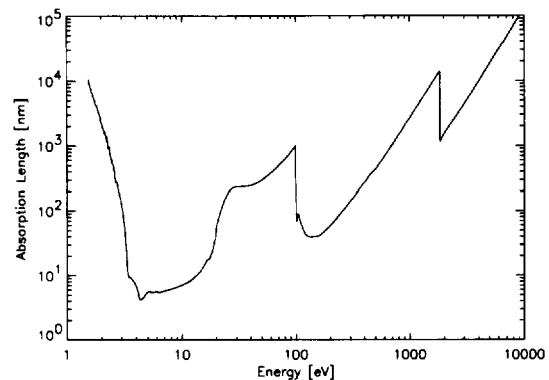


Fig. 1. Absorption length in silicon for photons of various wavelengths from X-ray to the infrared [5].

* Corresponding author. Tel.: +49 89 83940046; fax: +49 89 83940011; e-mail: roh@mpe-garching.mpg.de.

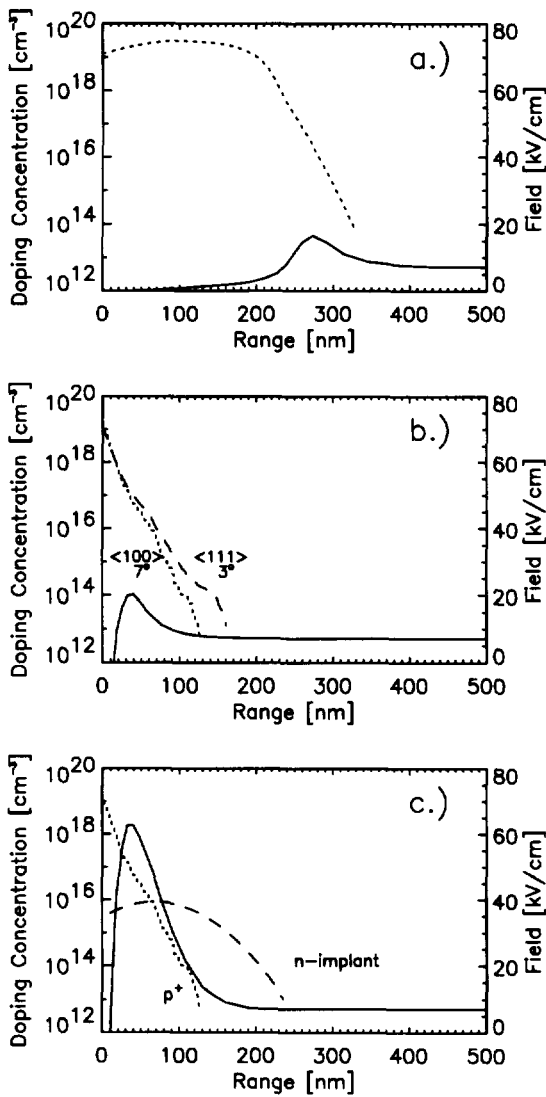


Fig. 2. Doping profiles (dotted lines) and electric fields (solid lines) for different entrance window implantations: (a) standard 12.5 keV boron into silicon (profile obtained by spreading resistance measurement), (b) same energy and dose of implanted boron atoms through a SiO₂ layer (for different wafer material and tilt angle during implantation), and (c) as before, plus an additional phosphorous implantation to increase the electric field.

$$\partial E / \partial x = q / \epsilon (p(x) - n(x) + N_D^+(x) - N_A^-(x)), \quad (1)$$

the maximum electric field strength is hardly affected by this technology. Placing an additional *n*-implant right behind the *p*⁺-implantation will result in an increase of the electric field according to the implanted phosphorus dose. The calculated doping profiles and corresponding electric field are shown in Fig. 2c. An increase in the electric field by a factor of three is achieved [2].

2. Measurements

2.1. Optical response

For a test of the optical response, as it is described in this paper, simple diodes with an area between 25 mm² and 300 mm² were used. The entrance side *pn*-junction was identically processed as for the drift detectors described later. The spectral responsivity was measured in the wavelength range between 200 nm and 800 nm. For a calibration of the absolute responsivity $R(\lambda)$, two Hamamatsu diodes were used, depending on the wavelength (AE-968 for wavelengths below 450 nm, 1790 for longer wavelengths). The spectral responsivity $R(\lambda)$ is related to the internal quantum efficiency $\epsilon(\lambda)$ as

$$R(\lambda) = (1 - \rho(\lambda))\epsilon(\lambda) \frac{\lambda e}{hc}, \quad (2)$$

where $\epsilon(\lambda)$ is the diode's internal quantum efficiency and $\rho(\lambda)$ the reflectance. While necessary for a determination of the internal quantum efficiency, measurements of the detector reflectance could not be performed yet.

In Fig. 3 are shown the results for detectors with different entrance window technologies. A maximum in the external quantum efficiency of 95% occurs for the detector with an ultrathin entrance window at a wavelength of 230 nm. This is exactly the threshold from one electron-hole pair generation to the generation of two electron-hole pairs. For photon energies below approximately 5 eV, one electron-hole pair is generated by a single photon, whereas above the process of generating two electron-hole pairs by one photon evolves. The obtained quantum efficiency implies a quantum gain in the UV region. The shallow *p*⁺-implantation requires a biasing of the detector. This is no disadvantage since the leakage current is less than 5 nA/cm² at full depletion (100 V) and only a small biasing voltage of approximately 1 V is required for operation.

The photosensitivity in the UV- and blue wavelength range for a conventionally processed detector is much lower. A substantial drop in the quantum efficiency occurs for wavelengths below 450 nm, corresponding to absorption lengths shorter than 250 nm. This is approximately the position of the *pn*-junction. Biasing the detector has only very little effect on the performance and is not necessary.

All detectors had no anti-reflection coating. The SiO₂ thicknesses were approximately 30 Å, which is the naturally grown oxide, for a detector with conventional processed entrance window and 200 Å for a ultrathin entrance windows.

2.2. X-ray performance

The absorption length of silicon shows a minimum of 40 nm for X-rays at 133 eV. Thus the charge collection

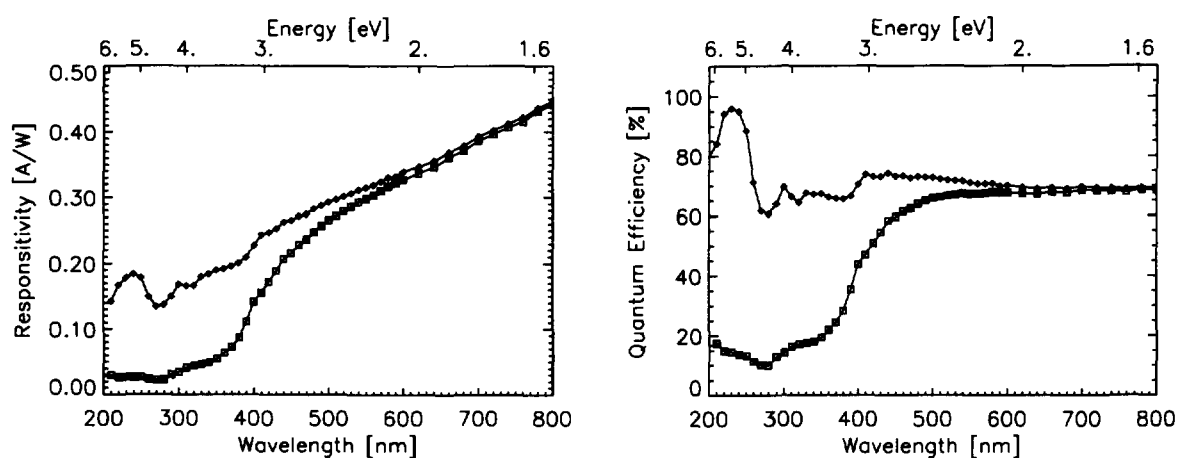


Fig. 3. Spectral responsivity and external quantum efficiency for two detectors with differently processed entrance windows. The SiO_2 thickness was approximately 30 \AA for a conventional (hollow squares) and 200 \AA for an ultrathin entrance window (filled squares). The detectors were operated at a bias voltage of 1 V.

efficiency (CCE) just beneath the detector surface plays a major role in the detector performance for X-ray spectroscopy as well as for optical measurements. A model to calculate detector response functions at various X-ray energies was deduced, taking account of the photon absorption process, the formation of a charge cloud of secondary electrons due to scattering processes of high energetic primary electrons, and a CCE as a function of detector parameters [1]. For each entrance window technology and type of detector material, one CCE-function explained the measured spectra over the entire range of energy.

Monoenergetic photons in the energy range between 150 eV and 1 keV were obtained at a soft X-ray beamline of the Physikalisch-Technische Bundesanstalt (PTB) at the electron storage ring BESSY in Berlin. Pulse-height distributions for various X-ray energies are shown in Fig. 4. The poorer performance of detectors on $\langle 111 \rangle$ -silicon material cannot be explained solely by a higher surface recombination velocity caused by a higher density of interface states at the Si– SiO_2 interface. The shape of the CCE depends on the carrier lifetime of electrons and is thus correlated with the spreading of the implantation profile. There are clues that the profile might reach farther into the bulk for $\langle 111 \rangle$ -silicon due to an enhanced channeling as a result of a smaller tilt angle during implantation [2].

Improvements in the detector performance are also represented by the peak to valley ratio for higher energetic photons. Table 1 shows the measured ratios for the $\text{Mn}_{K\alpha}$ line for different entrance window technologies.

2.3. α -particle measurements

An alternative access for an evaluation of charge losses at the detector entrance window is the so-called tilting

technique [4]. Two ^{241}Am α -sources hit the detector under different angles of incidence. The resulting difference in energy loss ΔE is reflected by pulses of different amplitudes. Assuming a simple geometric model, the effective entrance window thickness ΔX is obtained as

$$\Delta E = \Delta X \left(\frac{\partial E}{\partial X} \right)_{\text{Si}} \left(\frac{1}{\cos \theta} - 1 \right). \quad (3)$$

For a 5.486 MeV α -particle, the energy loss in a ‘‘dead’’-layer of 50 nm silicon ($\partial E/\partial X = 140 \text{ eV/nm}$) is $\Delta E = 7 \text{ keV}$ for normal incidence and $\Delta E' = 40.3 \text{ keV}$ for $\theta = 80^\circ$. Thus, the difference in the peak position of the two spectra is 33.3 keV. The spectrum obtained with two ^{241}Am α -sources under angles of incidence of 0° and 80° is shown in Fig. 5 for a detector with an entrance window width of 120 \AA . Table 2 gives an overview for the measured window thicknesses for different technologies.

As for measurements in the optical and X-ray region, the detector on $\langle 100 \rangle$ -silicon material shows superior results as well. Comparable results on a $\langle 111 \rangle$ detector are achieved with an enhanced field p^+n -junction. The effective entrance window thicknesses of 120 \AA correspond to the lowest values obtained for implanted pn -junction detectors so far.

3. The silicon drift detector

The silicon drift detector, in its basic form proposed by Gatti and Rehak [6], is a fully depleted detector in which signal charges are driven to the collecting anode by an electric field parallel to the surface. Fig. 6 gives a schematic cut through the detector. The n -type bulk is fully depleted from the p^+ rear contact, which acts as the radiation entrance window. On the opposite side, the negative bias of the p^+ rings increases from the first ring

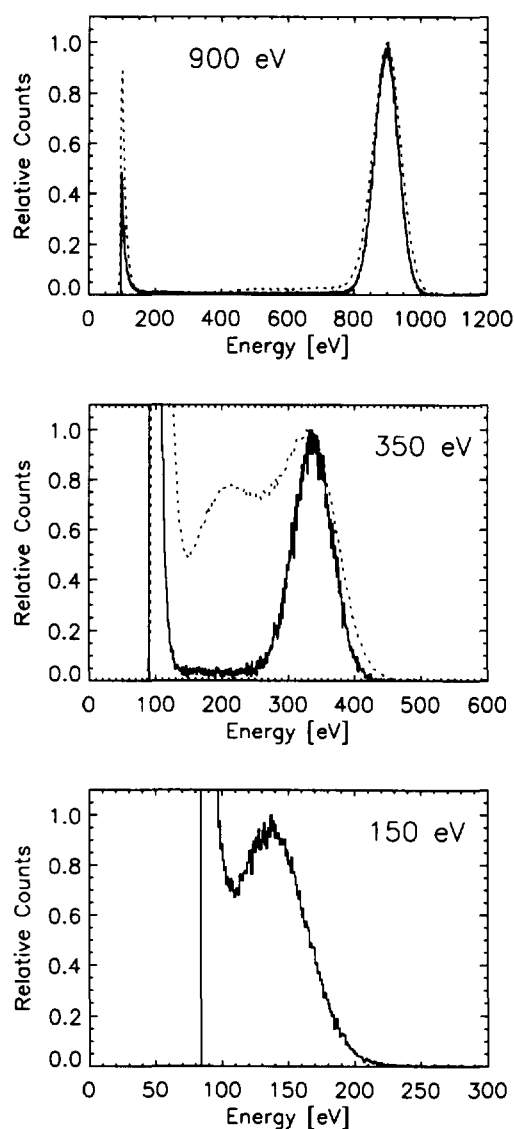


Fig. 4. Comparison of the normalized response functions of detectors produced on both $\langle 100 \rangle$ (straight lines) and $\langle 111 \rangle$ (dotted lines) high ohmic silicon material for photon energies varying from 150 to 900 eV. For X-ray energies below 350 eV, measurements of detectors on $\langle 111 \rangle$ material did not reveal a separable signal peak.

next to the anode to the outermost ring, creating a potential minimum for electrons which falls diagonally from the rear contact edge of the detector to the readout anode in the center. The outstanding feature of this detector concept is the extremely low output capacitance, which is independent of the detector area. To fully exploit this feature, a JFET is integrated on the detector chip to act as the first amplification stage. Stray capacitances due to various connections are minimized and a correct capacitive matching between detector and amplifier is achieved.

Table 1

Peak to valley ratios of $\text{Mn}_{\text{K}\alpha}$ line at 140 K for different wafer materials and backside implantations. The background value was calculated as the mean value of counts in an energy interval between 800 eV and 1200 eV

Material	Implantation	Peak to valley ratio
$\langle 111 \rangle / \langle 100 \rangle^a$	p^+	2100:1
$\langle 111 \rangle$	p^+ through SiO_2	3700:1
$\langle 100 \rangle$	p^+ through SiO_2	4300:1
$\langle 100 \rangle$	p^+ through $\text{SiO}_2 + n$	5700:1

^aNo difference in the spectral resolution was observed for detectors with a standard p^+ implantation on $\langle 111 \rangle$ and $\langle 100 \rangle$ silicon material.

Test detectors with a total area of 21 mm² have been fabricated, which were composed of six individual devices. A redesign is planned with a slightly improved topology, based on 5 mm² unit cells to be grouped in an array of up to 39 individual cells for a total detector area of almost 2 cm².

For the $\text{Mn}_{\text{K}\alpha}$ line of a radioactive ⁵⁵Fe-source, an energy resolution of 227 eV (FWHM) at room temperature (300 K) with shaping-times of 250–500 ns was achieved. For count rates higher than $8 \times 10^6 \text{ s}^{-1} \text{ cm}^{-2}$, the $\text{Mn}_{\text{K}\alpha}$ line is widened up to 250 eV and reached 350 eV for count rates around $3 \times 10^7 \text{ s}^{-1} \text{ cm}^{-2}$. By cooling the detector with a single stage Peltier cooling system, the spectroscopic resolution decreases to 152 eV at -20°C . At liquid nitrogen temperatures, the energy resolution is better than 140 eV.

The proposal of a multipurpose dosimeter for unknown radiation, covering an energy range up to 100 MeV, is shown in Fig. 7 [7]. The silicon drift detector can be used for photons and charged particles below 80 keV. For neutrons and high energy X-rays, a converter in front of the detector is needed. For photons above 80 keV, a

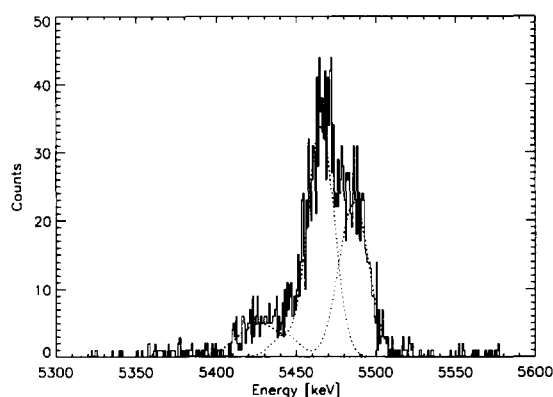


Fig. 5. ²⁴¹Am α -particle pulse-height spectrum at angles of incidence of 0° and 80° . The silicon entrance window is merely $(120 \pm 30) \text{ \AA}$, which confirms the excellent results of X-ray and optical measurements.

Table 2

Measured entrance window thicknesses with two ^{241}Am -sources and angles of incidence of 0° and 80° . The errors in determining the entrance window width are in the order of $\pm 15\text{--}20\%$ and are mainly caused by uncertainties in measuring the oxide thickness at the entrance window

Material	Implantation	Oxide thickness (\AA)	ΔE (keV)	ΔX_{total} (\AA)	ΔX_{Si} (\AA)
(111)	p^+	30	58.0	900	900
(111)	p^+ through SiO_2	250	35.2	550	300
(111)	p^+ through SiO_2	650	64.0	950	300
(100)	p^+ through SiO_2	200	20.6	320	120
(111)	p^+ through SiO_2 plus additional n	480	36.6	600	120

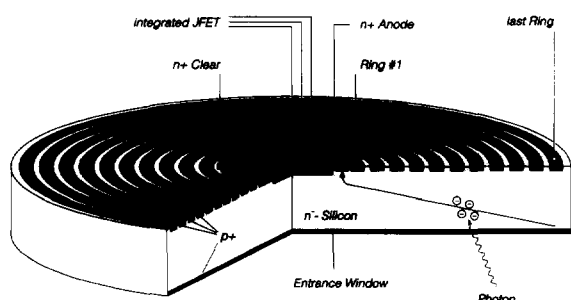


Fig. 6. Schematic cut through a silicon drift detector with an integrated JFET. The unstructured p^+ rear contact of the device acts as the radiation entrance window.

scintillating crystal (e.g. $\text{NaI}(\text{Ti})$, $\text{CsI}(\text{Ti})$ or BGO) is included. Due to the low noise of the solid state detector, the quality of measurements is limited only by the photon statistics of the scintillating material. Measurements can be performed in a single event detection mode with event rates up to $10^7 \text{ s}^{-1} \text{ cm}^{-2}$.

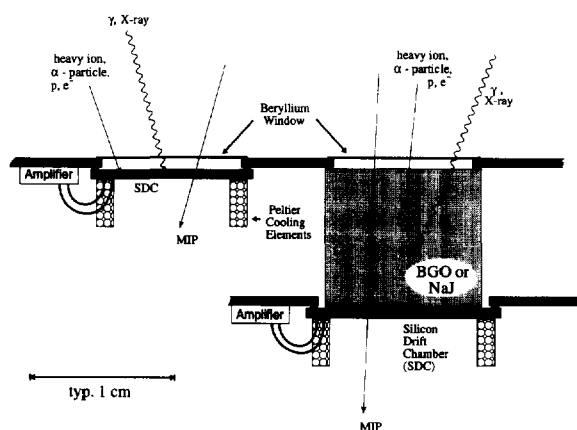


Fig. 7. Schematic drawing of a multipurpose dosimeter for unknown radiation. While the detector on the left hand side detects ionizing radiation up to 80 keV, the silicon drift detector in combination with a scintillator crystal measures radiation up to 100 MeV [7].

4. Conclusion

Large area silicon drift detectors have been developed and successfully tested. At temperatures, which are easily achieved by a simple Peltier cooling system their energy resolution approaches values of classical $\text{Si}(\text{Li})$ detectors at cryogenic temperatures. Due to the fact that the device operation is mostly independent of the entrance window technology, optimizations are easily implemented for specific needs, i.e. anti-reflection coatings for optical measurements.

The applied entrance window technology improves the spectroscopic resolution of detectors for all kinds of tested radiation. The obtained results are among the best reported so far for ion implanted silicon detectors.

Acknowledgement

The authors would like to thank the technology staff of the MPI Halbleiterlabor for their excellent work of producing the detector structures used in this work and D. Fuchs of the Physikalisch-Technische Bundesanstalt in Berlin for his support during the measurement period at BESSY. Financial support from Eurisys Mesures is gratefully acknowledged.

References

- [1] R. Hartmann, P. Lechner, L. Strüder, F. Scholze and G. Ulm, *Metrologia* 32 (1996) 491.
- [2] R. Hartmann et al., *Nucl. Instr. and Meth. A* 377 (1996) 191.
- [3] H. Bräuniger, C. v. Zanthier et al., *Metrologia* 32 (1996) 643.
- [4] T. Maisch, S. Kalbitzer et al., *Nucl. Instr. and Meth. A* 288 (1990) 19.
- [5] E.D. Palik, *Handbook of Optical Constants of Solids* (Academic Press, New York, 1985).
- [6] E. Gatti, and P. Rehak, *Nucl. Instr. and Meth. A* 225 (1984) 608.
- [7] L. Strüder and H. Soltau, *Radiat. Prot. Dos.* 61 (1995) 39.